

# Correlated Coulomb drag in capacitively coupled quantum-dot structures

Kristen Kaasbjerg\* and Antti-Pekka Jauho

Center for Nanostructured Graphene (CNG), Department of Micro- and Nanotechnology,  
Technical University of Denmark, DK-2800 Kgs. Lyngby, Denmark

(Dated: January 6, 2016)

We consider Coulomb drag in capacitively coupled quantum dots (QDs) — a bias-driven dot and an unbiased dot where transport is due to Coulomb mediated energy transfer drag. To this end, we develop a master-equation approach which accounts for energy-dependent lead couplings, and identify a mesoscopic Coulomb drag mechanism driven by *nonlocal* multi-electron tunneling processes. Our theory establishes the conditions for a nonzero drag as well as the direction of the drag current in terms of microscopic system parameters. Interestingly, the direction of the drag current is *not* determined by the drive current, but by an interplay between the energy-dependent lead couplings. Studying the drag mechanism in a graphene-based QD structure, we show that the predictions of our theory are consistent with recent experiments on Coulomb drag in such structures.

PACS numbers: 73.23.-b, 72.80.Vp, 73.23.Hk, 73.63.Kv

Electronic systems brought into close proximity may exhibit Coulomb drag [1, 2]: a current in one system induces a current (or a voltage) in a nearby undriven system. Importantly, the effect arises solely due to Coulomb interactions between the charge carriers in the two systems. Coulomb drag has been studied extensively in coupled two-dimensional systems, both experimentally [3–5] and theoretically [6–9], and has recently experienced a revival in one-dimensional systems [10–14] and graphene heterostructures [15–20].

In mesoscopic systems with broken translational invariance, e.g. quantum point contacts or quantum dots (QDs), momentum is not a good quantum number as in extended systems. Instead of momentum transfer, it is more natural to view *mesoscopic* Coulomb drag [21–23] as an interaction mediated energy transfer between the drive and the drag system. Such energy-transfer drag plays a central role in, for example, quantum measurements where a detector and a system exchange energy in a measurement on the system [24]. In this case, the drag can either constitute the signal in the detector generated by the measured quantum noise in the system [25–27], or be a disturbance in the system due to the measurement [28, 29], i.e. detector back-action.

In addition to energy transfer, Coulomb drag in capacitively coupled QDs (CQDs) relies on an asymmetry in the drag system [23]. This has been demonstrated in coupled double quantum dots [30], and recently in coupled single QDs [31, 32] where the asymmetry originates from the couplings to the leads. In the latter, Coulomb-drag effects beyond conventional mesoscopic QD drag [23, 33] were reported [31]. Not only are such effects of fundamental scientific interest, but they may also be important for the operating principles of novel QD devices [34–37].

In this work we provide a theoretical framework for the description of Coulomb drag in CQDs taking into account higher-order tunneling processes, and thereby going beyond conventional QD drag [23]. We uncover a drag

mechanism driven by *nonlocal* correlated multi-electron tunneling (cotunneling) processes. The drag stems from a ratchet mechanism where energy transfer is mediated by bias-induced switching between the CQD states at the honeycomb vertex of the stability diagram [38] sketched in Fig. 1(a). We identify both a cotunneling-only [arrow in Fig. 1(a)] and a cotunneling-assisted [circle in Fig. 1(a)] drag mechanism. In the latter, the system makes excursions around the triple point in the stability diagram like in charge pumping [39]. Our theory pinpoints the conditions for drag in terms of microscopic quantities and shows that the direction of the drag current is independent on the drive current and exhibits a nontrivial dependence on the lead couplings in the drag system.

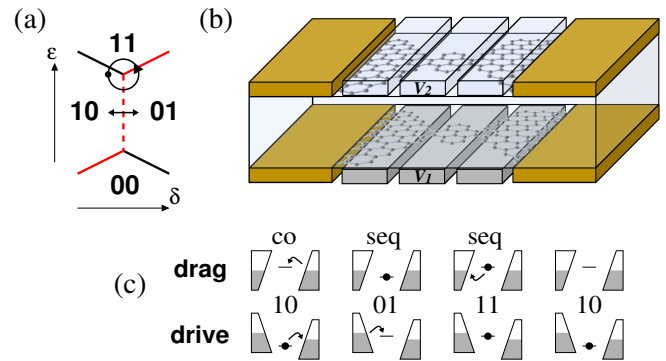


FIG. 1. (color online) (a) Stability diagram (honeycomb vertex) of two capacitively coupled QDs as a function of their gate detuning  $\delta = V_2 - V_1$  and common gate  $\epsilon = V_1 + V_2$ . (b) Illustration of a graphene-based CQD heterostructure with two QDs defined in stacked graphene layers separated by a thin isolating dielectric [31]. A series of top and bottom gates control the potentials on the quantum dots ( $V_{1/2}$ ) and their adjacent graphene leads. (c) Sequence of tunneling processes underlying the drag mechanism [closed circle in (a); see also Eq. (9)]. Energy-dependent lead couplings are essential to induce a directional drag current.

We demonstrate the rich properties of the drag mechanism by studying drag in the graphene-based CQD structure illustrated in Fig. 1(b). Such experimentally realizable graphene-based QD structures are unique due their large tunability [40–44], large interdot charging energies [31], and built-in graphene leads. We envision structures in which local gating allows to control the chemical potentials of the lead regions [45, 46] and create, e.g.,  $p$ -QD- $n$  junctions across the individual QDs. As we demonstrate below, this opens the opportunity to control the direction of the drag current. Finally, we elaborate on the role of the drag mechanism in the recently observed Coulomb drag in a graphene-based CQD structure [31].

**General model and theory.**—We consider a generic (spinless) model for two capacitively coupled QDs—a drive ( $i = 1$ ) and a drag ( $i = 2$ ) dot—with one level each,  $H_{\text{CQD}} = \sum_i \varepsilon_i n_i + U_{12} n_1 n_2$ , where the dot levels are controlled by gate voltages  $\varepsilon_i = -eV_i$ ,  $n_i = d_i^\dagger d_i$  is the dot occupation, and  $U_{12} = e^2/2C$  is the capacitive inter-dot coupling. The dots are coupled to separate source and drain contacts,  $H_\alpha = \sum_k \xi_{\alpha k} c_{\alpha k}^\dagger c_{\alpha k}$ ,  $\xi_{\alpha k} = \varepsilon_k - \mu_\alpha$  ( $\alpha = L_i, R_i$ ), via tunnel Hamiltonians  $H_T = \sum_{\alpha k} t_{\alpha k} c_{\alpha k}^\dagger d_i + \text{hc}$ . In contrast to the usual wide-band approximation where the lead couplings are assumed constant, we here consider energy-dependent couplings  $\Gamma_\alpha(\varepsilon) = 2\pi\rho_\alpha(\varepsilon)|t_\alpha(\varepsilon)|^2$ , where  $\rho_\alpha$  is the density of states (DOS) in lead  $\alpha$  and  $t_\alpha$  is the tunnel coupling. Like in conventional QD drag [23, 31], this is the key ingredient for the drag mechanism described below.

We describe the transport through the drive and drag dots with a master equation approach valid for  $k_B T \gtrsim \Gamma_\alpha$  [47]. The occupation probabilities  $p_m$  for the CQD states,  $|m\rangle = |n_1 n_2\rangle \in \{|00\rangle, |10\rangle, |01\rangle, |11\rangle\}$ , are determined by the rate equations

$$\dot{p}_m = -p_m \sum_{n \neq m} \Gamma_{mn} + \sum_{n \neq m} p_n \Gamma_{nm}, \quad (1)$$

which together with the normalization condition  $\sum_m p_m = 1$  are solved for the steady-state probabilities, i.e.  $\dot{p}_m = 0$ .

The rates for tunneling-induced transition between the states are obtained from the generalized Fermi golden rule [47],

$$\Gamma_{mn} = \frac{2\pi}{\hbar} \sum_{i'f'} W_{i'f'} |\langle f|T|i\rangle|^2 \delta(E_f - E_i). \quad (2)$$

Here,  $|i/f\rangle = |m/n\rangle \otimes |i'/f'\rangle$  are products of QD and lead states, the sum is over possible initial  $|i'\rangle$  and final  $|f'\rangle$  states of the leads,  $W_{i'f'}$  is the probability for the initial lead state  $|i'\rangle$ , and  $T = H_T + H_T G_0 H_T + \dots$  is the  $T$ -matrix with  $G_0 = \frac{1}{E_i - H_0}$  denoting the Green function in the absence of tunneling, i.e.  $H_0 = H_{\text{CQD}} + \sum_\alpha H_\alpha$ . The correlations between real and virtual occupations of the QDs in tunneling processes are fully accounted for in  $G_0$  which is treated exactly.

To lowest-order in the tunneling Hamiltonian, the transitions between the states are given by sequential tunneling processes with rates

$$\Gamma_{m,11}^\alpha = \hbar^{-1} \Gamma_\alpha(\Delta_{m,11}) f_\alpha(\Delta_{m,11}) \quad (3)$$

$$\Gamma_{m,00}^\alpha = \hbar^{-1} \Gamma_\alpha(\Delta_{m,00}) [1 - f_\alpha(\Delta_{m,00})] \quad (4)$$

$$\Gamma_{00,n}^\alpha = \hbar^{-1} \Gamma_\alpha(\Delta_{00,n}) f_\alpha(\Delta_{00,n}) \quad (5)$$

$$\Gamma_{11,n}^\alpha = \hbar^{-1} \Gamma_\alpha(\Delta_{11,n}) [1 - f_\alpha(\Delta_{11,n})], \quad (6)$$

where  $m, n \in \{10, 01\}$ ,  $f_\alpha$  is the Fermi function in lead  $\alpha$ , and  $\Delta_{mn} = E_n - E_m$ .

The next-to-leading order term in the  $T$ -matrix gives rise to *elastic* and *inelastic* cotunneling through the individual dots [48–50]. In addition, a *nonlocal* cotunneling process mediated by the capacitive inter-dot coupling arises. This is a correlated two-electron tunneling event in which the CQD switches between the  $10 \leftrightarrow 01$  states in one coherent process. The rate for nonlocal cotunneling processes which transfer an electron from lead  $\alpha$  to lead  $\beta$  is given by

$$\Gamma_{mn}^{\alpha\beta} = \int \frac{d\varepsilon}{2\pi\hbar} \Gamma_\alpha(\varepsilon + \Delta_{mn}) \Gamma_\beta(\varepsilon) f_\alpha(\varepsilon + \Delta_{mn}) [1 - f_\beta(\varepsilon)] \times \left| \frac{1}{\varepsilon - \Delta_{01,11}} - \frac{1}{\varepsilon + \Delta_{10,00}} \right|^2, \quad (7)$$

where  $m, n \in \{10, 01\}$  and the terms in the last line account for the energy of the virtually-occupied intermediate  $00/11$  states. To evaluate the cotunneling rates at finite temperature and bias, we have generalized the commonly applied regularization scheme [51, 52] to the situation with energy-dependent lead couplings [53].

From the solution to the master equation (1), the currents in the various leads are obtained as

$$I_\alpha = -e \sum_{mn} p_m (\Gamma_{mn}^{\rightarrow\alpha} - \Gamma_{mn}^{\alpha\rightarrow}), \quad (8)$$

where  $\Gamma^{\rightarrow\alpha}$  ( $\Gamma^{\alpha\rightarrow}$ ) denotes the rate for processes which transfer an electron into (out of) lead  $\alpha$ , and the drive and drag currents are defined as  $I_{\text{drive}} = I_{L_1} = -I_{R_1}$  and  $I_{\text{drag}} = I_{L_2} = -I_{R_2}$ , respectively.

**Drag mechanism.**—At the honeycomb vertex of the CQD stability diagram in Fig. 1(a), a current can pass through the *biased* drive dot ( $\mu_{L_1/R_1} = \pm eV_{\text{sd}}/2$ ; the drag dot is kept *unbiased* throughout) along the degeneracy lines where its occupation can fluctuate via sequential or cotunneling (full and dashed red lines, respectively). Fixing the gate voltages to, e.g., the point below the  $10/11$  degeneracy line at the upper triple point in Fig. 1(a), this involves the sequence of transitions

$$|10\rangle \xleftrightarrow{\text{co}} |01\rangle \xleftrightarrow{\text{seq}} |11\rangle \xleftrightarrow{\text{seq}} |10\rangle, \quad (9)$$

where, for  $eV_{\text{sd}} > \Delta_{mn} \gg k_B T$ , the two first transitions are open in both directions, whereas the third transition

is only open in the forward direction because the drag dot is unbiased. In addition to the drive current, this may induce a drag current via steps where the drag dot is repeatedly filled and emptied. This is possible via the first step alone (cotunneling-only drag), or through the full sequence (cotunneling-assisted drag) which is illustrated in Fig. 1(c). Note that the *nonlocal* cotunneling process is instrumental in both cases.

In order to generate a drag current, the drag dot must be filled and emptied at preferentially separate drag leads. This requires an asymmetry in the drag system. To identify the exact conditions, we expand the lead couplings around the equilibrium chemical potentials  $\mu_0$ ,  $\Gamma_\alpha(\varepsilon) \approx \Gamma_{\alpha 0} + \xi \partial \Gamma_\alpha$ , where  $\xi = \varepsilon - \mu_0$ ,  $\Gamma_{\alpha 0} = \Gamma_\alpha(\mu_0)$ , and  $\partial \Gamma_\alpha = \partial \Gamma_\alpha / \partial \varepsilon|_{\varepsilon=\mu_0}$ . Along the 10/01 degeneracy line,  $\Delta_{10,01} = 0$ , and in the nonlinear regime  $eV_{sd} \gg k_B T$  (but still  $eV_{sd} < U_{12}$ ) where the transport in the drive dot is *unidirectional*, we find for the drag current,

$$I_{\text{drag}} \sim \frac{\Gamma_{L_{10}} \Gamma_{R_{10}} (\Gamma_{L_{20}} \partial \Gamma_{R_{20}} - \Gamma_{R_{20}} \partial \Gamma_{L_{20}})}{\Gamma_{L_{20}} + \Gamma_{R_{20}}} F(V_{sd}), \quad (10)$$

where  $F(V_{sd}) = V_{sd}^2 \log V_{sd}$  away from (cotunneling-only) and at the triple points (cotunneling-assisted), respectively. The factor in parentheses in the numerator gives the conditions for drag. Notably, the drag is zero if the lead couplings of the drag dot are constant or differ by a multiplicative factor. Furthermore, the direction of the drag current is determined by two factors concerning the lead couplings to the drag dot: (i) their asymmetry, and (ii) their derivatives.

**Drag in graphene-based CQDs.**—In the following we study the drag effect in an idealized version of the graphene-based CQD structure illustrated in Fig 1(b). The QDs are assumed to be connected to bulk graphene leads with linear DOS,  $\rho_\alpha(\varepsilon) = \frac{g_s g_v}{2\pi(\hbar v_F)^2} |\varepsilon - E_{\alpha 0}|$ , which govern the energy dependence of the lead couplings, i.e.  $\Gamma_\alpha(\varepsilon) = 2\pi \rho_\alpha(\varepsilon) |t_\alpha|^2$  where  $t_\alpha$  is constant, and where the positions of the Dirac points in the leads,  $E_{\alpha 0} = -eV_\alpha$ , are controlled by local gates [see Fig. 3(a)]. This allows to tune both the strength of the lead couplings,  $\Gamma_{\alpha 0} \propto |\mu_0 - E_{\alpha 0}|$ , as well as their derivatives,  $\partial \Gamma_\alpha \gtrless 0$  on the upper/lower Dirac cones. In order to meet the conditions for a nonzero drag current,  $E_{L_{20}} \neq E_{R_{20}}$  like in Fig. 3(a) is necessary. Asymmetric tunnel couplings alone,  $t_{L_2} \neq t_{R_2} \rightarrow \Gamma_{L_2}(\varepsilon) \propto \Gamma_{R_2}(\varepsilon)$ , is not enough.

In Fig. 2(a),(c) we show the current through the drive and drag dots as a function of gate voltages for the situation in Fig. 3(a) with  $U_{12} > eV_{sd} \gg k_B T$ . The current through the drive dot in Fig. 2(a) is nonzero along the 00/10 and 01/11 degeneracy lines, and the 10/01 degeneracy line where it is dominated by, respectively, sequential tunneling and nonlocal cotunneling. In addition, elastic cotunneling through the drive dot appears as a background in the Coulomb-blockaded regions.

The induced drag current is shown in Fig. 2(c). A

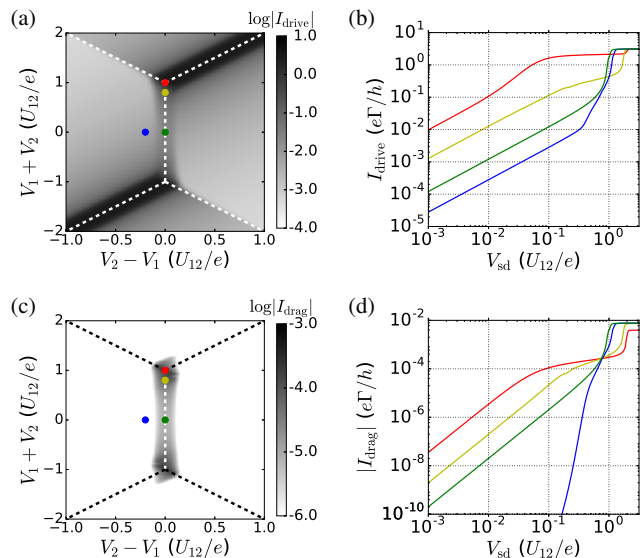


FIG. 2. (color online) Current through the drive (top) and drag (bottom) dots for the situation in Fig. 3(a). (a),(c) Current vs common gate and gate detuning with a bias voltage  $eV_{sd} = 0.2$  applied to the drive dot. (b),(d) Bias dependence of the drive and drag currents at the gate voltages  $(V_2 - V_1, V_1 + V_2)$  marked by dots in the left plots [red: (0.0, 1.0), yellow: (0.0, 0.8), green: (0.0, 0.0), blue: (-0.2, 0.0)]. Parameters (in units of  $U_{12}$ ):  $U_{12} = 1$ ,  $\Gamma_{L_{10}/R_{10}} = \Gamma_{L_{20}/R_{20}} = 0.01 \equiv \Gamma$ ,  $\partial \Gamma_{L_2} = -\partial \Gamma_{R_2}$ ,  $t_{L_2} = t_{R_2}$ ,  $k_B T = 0.01$ .

finite drag current is observed along the 10/01 degeneracy line where the nonlocal cotunneling channel is open. With the bias applied symmetrically in the drive dot, the drag region is limited by  $|\Delta_{10,01}| = e|V_2 - V_1| < eV_{sd}/2$  on the horizontal axis. Away from the triple points ( $|\Delta_{10,01,00/11}| \gg eV_{sd}$ ), the drag is driven solely by the nonlocal cotunneling process. In the vicinity of the upper (lower) triple point,  $eV_{sd} \gtrless |\Delta_{01,11}|$  ( $\Delta_{10,00}$ ), the bias on the drive dot opens the  $01 \leftrightarrow 11$  ( $10 \leftrightarrow 00$ ) transition via sequential tunneling, and the drag changes to cotunneling-assisted drag. This results in an enhanced drag current compared to the cotunneling-only drag.

Figure 2(b),(d) show the bias dependence of the drive and drag currents at the gate voltages marked by dots in Fig. 2(a),(c). In the linear low-bias regime,  $eV_{sd} < k_B T$ ,  $I_{\text{drive}} \propto V_{sd}$  and  $I_{\text{drag}} \propto V_{sd}^2$  for  $|\Delta_{10,01}| < k_B T$  (red, yellow and green dots). Away from the degeneracy line where  $|\Delta_{10,01}| > k_B T$  (blue dot), the nonlocal cotunneling process is exponentially suppressed,  $\Gamma_{10,01} \sim e^{-\Delta_{10,01}/k_B T}$ , resulting in a vanishing drag current. However, the drive current remains finite due to elastic cotunneling. In the nonlinear regime,  $eV_{sd} > k_B T$ ,  $I_{\text{drag}} \sim V_{sd}^2$  up to  $eV_{sd} \sim \max(2|\Delta_{10,01}|, |\Delta_{10,01,11}|)$  where it experiences a crossover to a  $I_{\text{drag}} \sim \log V_{sd}$  dependence in agreement with Eq. (10). At even higher bias,  $eV_{sd} \gtrsim U_{12}$ , the conventional drag mechanism [23] which is driven by sequential tunneling takes over (see also below).

From Eq. (10) it is clear that the direction of the drag

current depends, in a nontrivial way, on the lead couplings in the drag system. This is demonstrated in Fig. 3 which shows the drag current at the upper triple point as a function of the positions of the Dirac point in the drag leads. At the diagonal we have  $\Gamma_{L_2}(\varepsilon) = \Gamma_{R_2}(\varepsilon)$ , and hence the drag vanishes. Off the diagonal,  $\Gamma_{L_2} \neq \Gamma_{R_2}$  and  $\partial\Gamma_{L_2} = \partial\Gamma_{R_2}$ , the factor  $\Gamma_{L_2} - \Gamma_{R_2}$  governs the sign of the drag current. Upon crossing the Dirac point in one of the leads, the drag changes sign due to an inversion in the sign of the corresponding DOS derivative. Remarkably, the drag becomes independent on  $|\mu_0 - E_{L_2,0}/R_2|$  in this case. This follows from the fact that for symmetric tunnel couplings,  $\partial\Gamma_{L_2} = -\partial\Gamma_{R_2}$ , which leads to a cancellation of the  $\Gamma_{L_2} + \Gamma_{R_2}$  factors in Eq. (10). For asymmetric tunnel couplings this is not the case. The unconventional sign of the mesoscopic drag, which we have verified also holds for the conventional drag mechanism [23], is in stark contrast to that of the drag in coupled graphene layers [19].

In bias spectroscopy of CQDs, the drag mechanism leaves distinct fingerprints inside the so-called Coulomb-blockade diamonds where the sequential tunneling drive and drag currents are suppressed. Figure 4 shows the drive (top) and drag (bottom) currents at the center of the honeycomb vertex (green dot in Fig. 2) as a function of gate detuning and drive bias. In the low-bias Coulomb-blockaded regime,  $eV_{sd} < U_{12} + e|V_2 - V_1|$ , the drive current is dominated by elastic and nonlocal cotunneling, with the latter limited to the region  $V_{sd}/2 > |V_2 - V_1|$ . A cotunneling-driven drag current is observed in the same region.

At higher bias,  $eV_{sd} > U_{12} + e|V_2 - V_1|$ , the resonances to the 00 and 11 states enter the bias window, and sequential tunneling dominates both the drive and drag currents. However, outside the interval  $e|V_2 - V_1| < U_{12}$  on the horizontal axis, the sequential-tunneling driven drag mechanism is quenched [23], and the cotunneling-

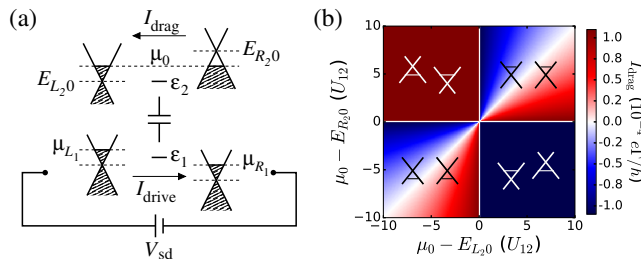


FIG. 3. (color online) (a) Energy level diagram of a graphene-based CQD where the QD levels,  $\varepsilon_i = -eV_i$ , and the positions of the Dirac points in the leads,  $E_{\alpha 0} = -eV_{\alpha}$ , are controlled by local gates [see also illustration in Fig. 1(b)]. (b) Drag current at the upper triple point as a function of gate voltage on the leads of the drag system (see Dirac cone insets). Parameters (in units of  $U_{12}$ ):  $U_{12} = 1$ ,  $\Gamma_{L_1,0}/R_1 = 0.01 \equiv \Gamma$ ,  $\Gamma_{L_2,0}/R_2 \propto |\mu_0 - E_{L_2,0}/R_2|$ ,  $\partial\Gamma_{L_2}/R_2 = \text{sgn}(\mu_0 - E_{L_2,0}/R_2)$ ,  $t_{L_2} = t_{R_2}$ ,  $eV_{sd} = 0.1$ ,  $k_B T = 0.01$ .

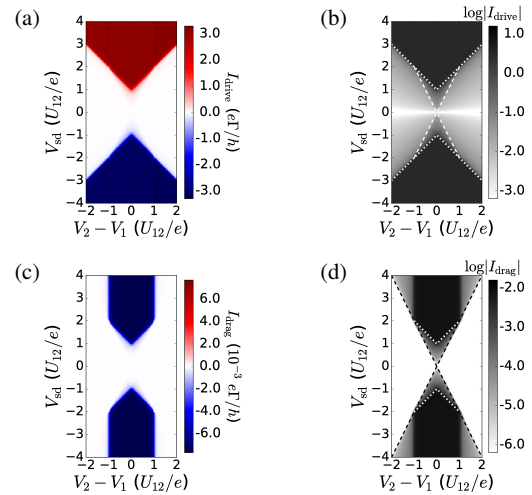


FIG. 4. (color online) Bias spectroscopy of the drive [(a),(b)] and drag [(c),(d)] dots at the center of the 10/01 degeneracy line and with the bias applied to the drive dot. (a),(c): linear scale. (b),(d): log scale. The dashed (dotted) lines mark the boundaries of the regions dominated by nonlocal cotunneling (sequential tunneling). See caption of Fig. 2 for parameters.

assisted mechanism takes over for  $eV_{sd}/2 > e|V_2 - V_1| > U_{12}$ . The different slopes  $s$  of the boundaries to the regions where, respectively, sequential tunneling (dotted,  $|s| = 1$ ) and nonlocal cotunneling (dashed,  $|s| = 2$ ) dominates the drive and drag currents (see log plots in Fig. 4), is a direct fingerprint of nonlocal cotunneling dominated transport [53].

Finally, we estimate the magnitude of the drag currents. Taking  $\Gamma_{\alpha}, k_B T \sim 0.1U_{12}$ , a drag current of the order of  $I_{\text{drag}} \gtrsim (U_{12}/\text{meV})^2$  pA [ $\gtrsim 0.1(U_{12}/\text{meV})^2$  nA] is predicted for cotunneling-assisted (sequential) drag for  $eV_{sd} \gtrsim k_B T$ ,  $\max(2|\Delta_{10,01}|, |\Delta_{10/01,00/11}|) (\gtrsim U_{12})$ . The cotunneling-driven drag is thus well within experimentally detectable currents, and its signatures in bias spectroscopy have recently been observed experimentally in Ref. 31.

**Conclusions.**—In summary, we have identified a ratchet-like drag mechanism in CQDs driven by nonlocal cotunneling processes. The key ingredient for the drag mechanism is that the coupling to the leads be energy dependent. This can be achieved via, e.g., gate-dependent tunnel barriers [36, 55], or be intrinsic to the QD system as in graphene-based quantum-dot structures with built-in graphene leads [31]. Studying Coulomb drag in an idealized version of such a QD structure, we demonstrated the nontrivial dependence of the drag current on the lead couplings and its fingerprints in bias spectroscopy. Possible routes for future explorations of drag in CQDs include shot noise and cross correlations characteristics [23, 56, 57], the effect of level broadening [58, 59] and Kondo physics [60, 61] which become important at  $\Gamma_{\alpha} > k_B T$ , as well as drag due to other coupling mecha-

nisms between the QDs [62].

**Acknowledgements.**—We would like to thank J. Santos and N. A. Mortensen for fruitful discussions, and K. Ensslin and D. Bischoff for clarifications on the experimental details in Ref. 31 and comments on the manuscript. The Center for Nanostructured Graphene (CNG) is sponsored by the Danish Research Foundation, Project DNRF58.

---

\* cosby@fys.ku.dk

- [1] A. G. Rojo, “Electron-drag effects in coupled electron systems,” *J. Phys.: Condens. Matter* **11**, R31 (1999).
- [2] B. N. Narozhny and A. Levchenko, “Coulomb drag,” *Rev. Mod. Phys.* **XXX**, XXX (2016), accepted.
- [3] P. M. Solomon, P. J. Price, D. J. Frank, and D. C. La Tulipe, “New phenomena in coupled transport between 2D and 3D electron-gas layers,” *Phys. Rev. Lett.* **63**, 2508 (1989).
- [4] T. J. Gramila, J. P. Eisenstein, A. H. MacDonald, L. N. Pfeiffer, and K. W. West, “Mutual friction between parallel two-dimensional electron systems,” *Phys. Rev. Lett.* **66**, 1216 (1991).
- [5] U. Sivan, P. M. Solomon, and H. Shtrikman, “Coupled electron-hole transport,” *Phys. Rev. Lett.* **68**, 1196 (1992).
- [6] A.-P. Jauho and H. Smith, “Coulomb drag between parallel two-dimensional electron systems,” *Phys. Rev. B* **47**, 4420 (1993).
- [7] K. Flensberg and B. Yu-Kuang Hu, “Coulomb drag as a probe of coupled plasmon modes in parallel quantum wells,” *Phys. Rev. Lett.* **73**, 3572 (1994).
- [8] K. Flensberg, B. Yu-Kuang Hu, A.-P. Jauho, and J. M. Kinaret, “Linear-response theory of Coulomb drag in coupled electron systems,” *Phys. Rev. B* **52**, 14761 (1995).
- [9] A. Kamenev and Y. Oreg, “Coulomb drag in normal metals and superconductors: Diagrammatic approach,” *Phys. Rev. B* **52**, 7516 (1995).
- [10] N. A. Mortensen, K. Flensberg, and A.-P. Jauho, “Mesoscopic fluctuations of Coulomb drag between quasiballistic one-dimensional wires,” *Phys. Rev. B* **65**, 085317 (2002).
- [11] M. Yamamoto, M. Stopa, Y. Tokura, Y. Hirayama, and S. Tarucha, “Negative Coulomb drag in a one-dimensional wire,” *Science* **313**, 204 (2006).
- [12] D. Laroche, G. Gervais, M. P. Lilly, and J. L. Reno, “Positive and negative Coulomb drag in vertically integrated one-dimensional quantum wires,” *Nature Nanotech.* **6**, 793 (2011).
- [13] D. Laroche, G. Gervais, M. P. Lilly, and J. L. Reno, “1D-1D Coulomb drag signature of a Luttinger liquid,” *Science* **343**, 631 (2014).
- [14] A. A. Shylau and A.-P. Jauho, “Plasmon-mediated Coulomb drag between graphene waveguides,” *Phys. Rev. B* **89**, 165421 (2014).
- [15] W.-K. Tse, B. Yu-Kuang Hu, and S. Das Sarma, “Theory of Coulomb drag in graphene,” *Phys. Rev. B* **76**, 081401(R) (2007).
- [16] E. H. Hwang, R. Sensarma, and S. Das Sarma, “Coulomb drag in monolayer and bilayer graphene,” *Phys. Rev. B* **84**, 245441 (2011).
- [17] S. Kim, I. Jo, J. Nah, Z. Yao, S. K. Banerjee, and E. Tutuc, “Coulomb drag of massless fermions in graphene,” *Phys. Rev. B* **83**, 161401(R) (2011).
- [18] M. I. Katsnelson, “Coulomb drag in graphene single layers separated by a thin spacer,” *Phys. Rev. B* **84**, 041407(R) (2011).
- [19] R. V. Gorbachev, A. K. Geim, M. I. Katsnelson, K. S. Novoselov, T. Tudorovskiy, I. V. Grigorieva, A. H. MacDonald, S. V. Morozov, K. Watanabe, T. Taniguchi, and L. A. Ponomarenko, “Strong Coulomb drag and broken symmetry in double-layer graphene,” *Nature Phys.* **8**, 896 (2012).
- [20] J. C. W. Song, D. A. Abanin, and L. S. Levitov, “Coulomb drag mechanisms in graphene,” *Nano. Lett.* **13**, 3631 (2013).
- [21] N. A. Mortensen, K. Flensberg, and A.-P. Jauho, “Coulomb drag in coherent mesoscopic systems,” *Phys. Rev. Lett.* **86**, 1841 (2001).
- [22] A. Levchenko and A. Kamenev, “Coulomb drag in quantum circuits,” *Phys. Rev. Lett.* **101**, 216806 (2008).
- [23] R. Sánchez, R. López, D. Sánchez, and M. Büttiker, “Mesoscopic Coulomb drag, broken detailed balance, and fluctuation relations,” *Phys. Rev. Lett.* **104**, 076801 (2010).
- [24] A. A. Clerk, M. H. Devoret, S. M. Girvin, F. Marquardt, and R. J. Schoelkopf, “Introduction to quantum noise, measurement, and amplification,” *Rev. Mod. Phys.* **82**, 1155 (2010).
- [25] R. Aguado and L. P. Kouwenhoven, “Double quantum dots as detectors of high-frequency quantum noise in mesoscopic conductors,” *Phys. Rev. Lett.* **84**, 1986 (2000).
- [26] E. Onac, F. Balestro, L. H. Willems van Beveren, U. Hartmann, Y. V. Nazarov, and L. P. Kouwenhoven, “Using a quantum dot as a high-frequency shot noise detector,” *Phys. Rev. Lett.* **96**, 176601 (2006).
- [27] S. Gustavsson, M. Studer, R. Leturcq, T. Ihn, K. Ensslin, D. C. Driscoll, and A. C. Gossard, “Frequency-selective single-photon detection using a double quantum dot,” *Phys. Rev. Lett.* **99**, 206804 (2007).
- [28] V. S. Khrapai, S. Ludwig, J. P. Kotthaus, H. P. Tranitz, and W. Wegscheider, “Double-dot quantum ratchet driven by an independently biased quantum point contact,” *Phys. Rev. Lett.* **97**, 176803 (2006).
- [29] D. Harbusch, D. Taubert, H. P. Tranitz, W. Wegscheider, and S. Ludwig, “Phonon-mediated versus Coulombic backaction in quantum dot circuits,” *Phys. Rev. Lett.* **104**, 196801 (2010).
- [30] G. Shinkai, T. Hayashi, T. Ota, K. Muraki, and T. Fujisawa, “Bidirectional current drag induced by two-electron cotunneling in coupled double quantum dots,” *Appl. Phys. Express* **2**, 081101 (2009).
- [31] D. Bischoff, M. Eich, O. Zilberberg, C. Rössler, T. Ihn, and K. Ensslin, “Measurement back-action in stacked graphene quantum dots,” *Nano. Lett.* **15**, 6003 (2015).
- [32] C. Volk, S. Engels, C. Neumann, and C. Stampfer, “Back action of graphene charge detectors on graphene and carbon nanotube quantum dots,” *XXX XXX*, XXX (2015), arXiv:1508.05193.
- [33] M. E. Raikh and F. von Oppen, “Coulomb drag for strongly localized electrons: A pumping mechanism,” *Phys. Rev. Lett.* **89**, 106601 (2002).

- [34] R. Sánchez and M. Büttiker, “Optimal energy quanta to current conversion,” *Phys. Rev. B* **83**, 085428 (2011).
- [35] B. Sothmann, R. Sánchez, and A. N. Jordan, “Thermoelectric energy harvesting with quantum dots,” *Nanotechnology* **26**, 032001 (2014).
- [36] H. Thierschmann, R. Sánchez, B. Sothmann, F. Arnold, C. Heyn, W. Hansen, H. Buhmann, and L. W. Molenkamp, “Three-terminal energy harvester with coupled quantum dots,” *Nature Nanotech.* **10**, 854 (2015).
- [37] J. V. Koski, A. Kutvonen, I. M. Khaymovich, T. AlaNissila, and J. P. Pekola, “On-chip Maxwell’s demon as an information-powered refrigerator,” *Phys. Rev. Lett.* **115**, 260602 (2015).
- [38] W. G. van der Wiel, S. De Franceschi, J. M. Elzerman, T. Fujisawa, S. Tarucha, and L. P. Kouwenhoven, “Electron transport through double quantum dots,” *Rev. Mod. Phys.* **75**, 1 (2003).
- [39] M. R. Connolly, K. L. Chiu, S. P. Giblin, M. Kataoka, J. D. Fletcher, C. Chua, J. P. Griffiths, G. A. C. Jones, V. I. Fal’ko, C. G. Smith, and T. J. B. M. Janssen, “Gigahertz quantized charge pumping in graphene quantum dots,” *Nature Nanotech.* **8**, 417 (2013).
- [40] L. A. Ponomarenko, F. Schedin, M. I. Katsnelson, R. Yang, E. W. Hill, K. S. Novoselov, and A. K. Geim, “Chaotic Dirac billiard in graphene quantum dots,” *Science* **320**, 356 (2008).
- [41] C. Stampfer, J. Güttinger, F. Molitor, D. Graf, T. Ihn, and K. Ensslin, “Tunable Coulomb blockade in nanostructured graphene,” *Appl. Phys. Lett.* **92**, 012102 (2008).
- [42] L.-J. Wang, G. Cao, T. Tu, H.-O. Li, C. Zhou, X.-J. Hao, Z. Su, G.-C. Guo, G.-P. Guo, and H.-W. Jiang, “A graphene quantum dot with a single electron transistor as integrated charge sensor,” *Appl. Phys. Lett.* **97**, 262113 (2010).
- [43] J. Güttinger, F. Molitor, C. Stampfer, S. Schnez, A. Jacobsen, S. Dröscher, and T. Ihn and K. Ensslin, “Transport through graphene quantum dots,” *Rep. Prog. Phys.* **75**, 126502 (2012).
- [44] D. Bischoff, A. Varlet, P. Simonet, M. Eich, H. C. Overweg, T. Ihn, and K. Ensslin, “Localized charge carriers in graphene nanodevices,” *Appl. Phys. Rev.* **2**, 031301 (2015).
- [45] B. Huard, J. A. Sulpizio, N. Stander, K. Todd, B. Yang, and D. Goldhaber-Gordon, “Transport measurements across a tunable potential barrier in graphene,” *Phys. Rev. Lett.* **98**, 236803 (2007).
- [46] B. Özyilmaz, P. Jarillo-Herrero, D. Efetov, D. A. Abanin, L. S. Levitov, and P. Kim, “Electronic transport and quantum Hall effect in bipolar graphene  $p-n-p$  junctions,” *Phys. Rev. Lett.* **99**, 166804 (2007).
- [47] H. Bruus and K. Flensberg, *Many-body Quantum Theory in Condensed Matter Physics* (Oxford University Press, 2004).
- [48] D. V. Averin and Yu. V. Nazarov, “Virtual electron diffusion during quantum tunneling of the electric charge,” *Phys. Rev. Lett.* **65**, 2446 (1990).
- [49] A. Furusaki and K. A. Matveev, “Theory of strong inelastic cotunneling,” *Phys. Rev. B* **52**, 16676 (1995).
- [50] S. De Franceschi, S. Sasaki, J. M. Elzerman, W. G. van der Wiel, S. Tarucha, and L. P. Kouwenhoven, “Electron cotunneling in a semiconductor quantum dot,” *Phys. Rev. Lett.* **86**, 878 (2001).
- [51] M. Turek and K. A. Matveev, “Cotunneling thermopower of single electron transistors,” *Phys. Rev. B* **65**, 115332 (2002).
- [52] J. Koch, F. von Oppen, Y. Oreg, and E. Sela, “Thermopower of single-molecule devices,” *Phys. Rev. B* **70**, 195107 (2004).
- [53] Supplemental material which includes (i) a detailed account of the cotunneling regularization scheme generalized to situations with energy-dependent lead couplings, (ii) results for the bias spectroscopy with an asymmetrically biased drive dot, and (iii) the additional Ref. [54].
- [54] M. Abramowitz and I. A. Stegun, *Handbook of Mathematical Functions with Formulas, Graphs, and Mathematical Tables*, 10th ed. (Dover, New York, 1964).
- [55] J. Waissman, M. Honig, S. Pecker, A. Benyamini, A. Hamo, and S. Ilani, “Realization of pristine and locally tunable one-dimensional electron systems in carbon nanotubes,” *Nature Nanotech.* **8**, 569 (2013).
- [56] D. T. McClure, L. DiCarlo, Y. Zhang, H.-A. Engel, C. M. Marcus, M. P. Hanson, and A. C. Gossard, “Tunable noise cross correlations in a double quantum dot,” *Phys. Rev. Lett.* **98**, 056801 (2007).
- [57] K. Kaasbjerg and W. Belzig, “Full counting statistics and shot noise of cotunneling in quantum dots and single-molecule transistors,” *Phys. Rev. B* **91**, 235413 (2015).
- [58] A. Thielmann, M. H. Hettler, J. König, and G. Schön, “Cotunneling current and shot noise in quantum dots,” *Phys. Rev. Lett.* **95**, 146806 (2005).
- [59] O. Zilberberg, A. Carmi, and A. Romito, “Measuring cotunneling in its wake,” *Phys. Rev. B* **90**, 205413 (2014).
- [60] V. Koerting, P. Wölffe, and J. Paaske, “Transconductance of a double quantum dot system in the Kondo regime,” *Phys. Rev. Lett.* **99**, 036807 (2007).
- [61] S. Amasha, A. J. Keller, I. G. Rau, A. Carmi, J. A. Katine, H. Shtrikman, Y. Oreg, and D. Goldhaber-Gordon, “Pseudospin-resolved transport spectroscopy of the Kondo effect in a double quantum dot,” *Phys. Rev. Lett.* **110**, 046604 (2013).
- [62] G.-W. Deng, D. Wei, S.-X. Li, J. R. Johansson, W.-C. Kong, H.-O. Li, G. Cao, M. Xiao, G.-C. Guo, F. Nori, H.-W. Jiang, and G.-P. Guo, “Coupling two distant double quantum dots with a microwave resonator,” *Nano. Lett.* **15**, 6620 (2015).

# Supplemental material for “*Correlated Coulomb drag in capacitively coupled quantum-dot structures*”

Kristen Kaasbjerg\* and Antti-Pekka Jauho

Center for Nanostructured Graphene (CNG), Department of Micro- and Nanotechnology,  
Technical University of Denmark, DK-2800 Kgs. Lyngby, Denmark

(Dated: December 30, 2015)

## S1. BIAS SPECTROSCOPY WITH THE BIAS VOLTAGE APPLIED ASYMMETRICALLY

In experiments, the bias voltage on the drive system is often applied to the source, or the drain, electrode only. In order to ease the comparison with our theoretically calculated bias spectroscopy diagrams (Fig. 4 of the main text where the bias has been applied symmetrically to the source and drain electrodes) we give in Fig. S1 the results for an asymmetrically applied bias voltage, i.e.  $\mu_{L_1} = eV_{sd} + \mu_0$  and  $\mu_{R_1} = \mu_0$ .

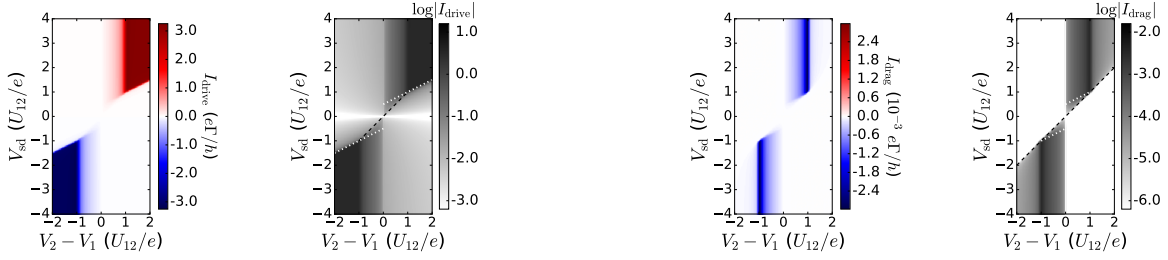


FIG. S1. (Color online) Current through the drive (left) and drag (right) dots at the center of the 10/01 degeneracy line vs bias and gate detuning with the bias on the drive dot applied asymmetrically, i.e.  $\mu_{L_1} = eV_{sd}$  and  $\mu_{R_1} = 0$ . Parameters (in units of  $U_{12}$ ):  $U_{12} = 1$ ,  $\Gamma_{L_{10}/R_{10}} = \Gamma_{L_{20}/R_{20}} = 0.01 \equiv \Gamma$ ,  $\partial\Gamma_{L_2} = -\partial\Gamma_{R_2}$ ,  $t_{L_2} = t_{R_2}$ ,  $k_B T = 0.01$ .

The main difference between the bias spectroscopy diagrams in Fig. 4 of the main text and those in Fig. S1 above, is the suppression of the currents at negative (positive) detuning,  $V_2 - V_1$ , and positive (negative) bias polarity. Furthermore, the slopes  $s$  of the boundaries to the regions where, respectively, sequential tunneling (dotted,  $|s| = 1/2$ ) and nonlocal cotunneling (dashed,  $|s| = 1$ ) dominates the drive and drag currents (see log plots in Fig. S1) are different.

Interestingly, we note that a feature similar to the one in the low-bias cotunneling-dominated drag current in the rightmost plot of Fig. S1, has been observed in the transconductance of two capacitively coupled QDs in Ref. 1 [their Fig. 4(g)].

## S2. COTUNNELING REGULARIZATION SCHEME

In this section, we generalize the commonly applied cotunneling regularization scheme<sup>2,3</sup> to the situation where the lead couplings are energy dependent. The result obtained here applies to general energy-dependent lead couplings which may originate from the either the lead density of states (DOS) and/or the tunnel couplings to the leads (see below). Furthermore, the generic form for the cotunneling rates considered below, allows for a straight-forward generalization to cotunneling in other QD systems.

From a  $T$ -matrix calculation<sup>4</sup> of cotunneling in the QD system considered in the main text, the rate for transferring an electron from lead  $\alpha$  to lead  $\beta$  in a cotunneling process (*elastic* or *nonlocal*) which, at the same time, changes the QD state from  $|m\rangle$  to  $|n\rangle$  ( $|m\rangle = |n\rangle$  for *elastic* cotunneling) can be written on the generic form

$$\begin{aligned} \Gamma_{mn}^{\alpha\beta} &= \int \frac{d\varepsilon}{2\pi\hbar} \Gamma_\alpha(\varepsilon + \Delta_{mn}) \Gamma_\beta(\varepsilon) \left| \frac{A}{\varepsilon - \Delta_1} + \frac{B}{\varepsilon - \Delta_2} \right|^2 f_\alpha(\varepsilon + \Delta_{mn}) [1 - f_\beta(\varepsilon)] \\ &= n_B(\mu_\beta - \mu_\alpha + \Delta_{mn}) \int \frac{d\varepsilon}{2\pi\hbar} \Gamma_\alpha(\varepsilon + \Delta_{mn}) \Gamma_\beta(\varepsilon) \left| \frac{A}{\varepsilon - \Delta_1} + \frac{B}{\varepsilon - \Delta_2} \right|^2 [f_\beta(\varepsilon) - f_\alpha(\varepsilon + \Delta_{mn})]. \end{aligned} \quad (S1)$$

Here,  $\Delta_{1,2}$  denotes the energy differences associated with the two possible intermediate states and  $A, B = \pm 1$  for electron- and hole-like intermediate states, respectively. Furthermore,  $\Gamma_\alpha(\varepsilon) = 2\pi\rho_\alpha(\varepsilon)|t_\alpha(\varepsilon)|^2$  is the *energy-dependent* lead coupling,  $\rho_\alpha$  is the density of states (DOS) in lead  $\alpha$ ,  $t_\alpha$  is the tunneling amplitude,  $\Delta_{mn} = E_n - E_m$  is the

energy difference between the initial and final states,  $f_\alpha$  is the Fermi function of lead  $\alpha$  with chemical potential  $\mu_\alpha$ , and  $n_B$  is the Bose-Einstein distribution. In the last equality, we have recast the integrand into a form that is easier to tackle.

In the expression for the cotunneling rate above, the energy denominators associated with the virtually-occupied intermediate states give rise to a diverging cotunneling rate when the intermediate states go ‘‘on-shell’’. To deal with this divergence, we follow the standard regularization scheme<sup>2,3</sup> and introduce a phenomenological tunnel broadening of the QD states (not accounted for in a  $T$ -matrix calculation) by adding an imaginary infinitesimal  $i\gamma$  (regularizer) in the energy denominators. The integral can then be evaluated after which the regularized cotunneling rates are obtained by taking the limit  $\gamma \rightarrow 0$ .

### A. General expression for the regularized cotunneling rates

With the regularizer added in the energy denominators of Eq. (S1), the cotunneling rate can be expressed as

$$\Gamma_{mn}^{\alpha\beta} = \frac{n_B(\mu_\beta - \mu_\alpha + \Delta_{mn})}{2\pi\hbar} \lim_{\gamma \rightarrow 0} \left[ A^2 I_1(\Delta_1) + B^2 I_1(\Delta_2) + 2AB I_2(\Delta_1, \Delta_2) \right] \quad (\text{S2})$$

where the integrals  $I_{1/2}$  are given by (with their  $\Delta_n$  dependence suppressed in the following)

$$I_n = \int_{-\infty}^{\infty} d\varepsilon \Gamma_\alpha(\varepsilon + \Delta_{mn}) \Gamma_\beta(\varepsilon) F_n(\varepsilon) [f_\beta(\varepsilon) - f_\alpha(\varepsilon + \Delta_{mn})], \quad (\text{S3})$$

and the functions  $F_n$  are defined by the terms which result from the absolute-value squared factor,

$$\begin{aligned} \left| \frac{A}{\varepsilon - \Delta_1 + i\gamma} + \frac{B}{\varepsilon - \Delta_2 + i\gamma} \right|^2 &= \left| \frac{A}{\varepsilon - \Delta_1 + i\gamma} \right|^2 + \left| \frac{B}{\varepsilon - \Delta_2 + i\gamma} \right|^2 + 2\text{Re} \left( \frac{A}{\varepsilon - \Delta_1 + i\gamma} \frac{B}{\varepsilon - \Delta_2 - i\gamma} \right) \\ &\equiv A^2 F_1(\varepsilon; \Delta_1) + B^2 F_1(\varepsilon; \Delta_2) + 2AB F_2(\varepsilon; \Delta_1, \Delta_2). \end{aligned} \quad (\text{S4})$$

This leaves us with two types of integrals,  $I_{1,2}$ , to evaluate.

We proceed to evaluate the integrals in Eq. (S3) using contour integration. To this end, we start by rewriting the Fermi functions as

$$f_\alpha(\varepsilon) = \frac{1}{2} \left[ 1 - \tanh \left( \frac{\varepsilon - \mu_\alpha}{2k_B T} \right) \right] = \frac{1}{2} \left[ 1 + \frac{i}{\pi} [\Psi_\alpha^+(\varepsilon) - \Psi_\alpha^-(\varepsilon)] \right], \quad (\text{S5})$$

where

$$\Psi_\alpha^\pm(\varepsilon) = \Psi \left( 1/2 \pm i \frac{\beta}{2\pi} (\varepsilon - \mu_\alpha) \right), \quad (\text{S6})$$

$\Psi$  is the digamma function<sup>5</sup>, and  $\beta = 1/k_B T$ . The two digamma functions  $\Psi^\pm$  have poles  $z_n = \mu_\alpha \pm i2\pi/\beta (n + \frac{1}{2})$ ,  $n \in \mathbb{N}$ , which lie in the positive and negative complex half-planes, respectively. We therefore split up the integral into two subintegrals,  $I_n = I_n^+ - I_n^-$ , which deal with the contributions from  $\Psi^\pm$  separately,

$$I_n^\pm = \frac{i}{2\pi} \int_{-\infty}^{\infty} d\varepsilon \Gamma_\alpha(\varepsilon + \Delta_{mn}) \Gamma_\beta(\varepsilon) F_n(\varepsilon) [\Psi_\beta^\pm(\varepsilon) - \Psi_\alpha^\pm(\varepsilon + \Delta_{mn})]. \quad (\text{S7})$$

This has the advantage that upon extending the integrations to closed contours in the complex plane, the poles of the  $\Psi^\pm$  functions can be avoided by closing the contours in the half plane where  $\Psi^\pm$  do not have any poles. If the lead couplings  $\Gamma_{\alpha/\beta}$  are well-behaved functions without singularities, the resulting contour integrals  $I_{cn}^\pm$  are thus given by the sum over residues of the integrand at the poles  $z_i$  of  $F_n$  which are enclosed by the integration contours,

$$I_{cn}^\pm = \frac{i}{2\pi} \oint_{C_\mp} dz \Gamma_\alpha(z + \Delta_{mn}) \Gamma_\beta(z) F_n(z) [\Psi_\beta^\pm(z) - \Psi_\alpha^\pm(z + \Delta_{mn})] = 2\pi i \sum_i \text{Res}(z_i). \quad (\text{S8})$$

Here, the contours are chosen as semicircles  $C_\mp$  with radius  $R \rightarrow \infty$  closed in the negative/positive complex half-planes, respectively (see Fig. S2).

Writing the contour integrals as a sum over the different contributions from the integration contour,

$$I_{cn}^\pm = \mp I_n^\pm + I_{C_{R\mp}}^\pm, \quad (\text{S9})$$



where  $\mp$  in front of the first term accounts for the direction of the contour along the real axis and  $I_{C_{R\mp}}^{\pm}$  denote the contribution from the semi-circle arcs, the integrals along the real axis in Eq. (S3) can be obtained as

$$I_n = I_n^+ - I_n^- = I_{C_{R_-}^+}^+ + I_{C_{R_+}^-}^- - I_{cn}^+ - I_{cn}^- \equiv I_{C_{Rn}} - I_{cn}. \quad (\text{S10})$$

In the following subsections, we evaluate the different contributions to the  $I_{1/2}$  integrals one by one. The contributions from the semi-circle arcs  $C_{R_{\pm}}$  need special attention since they, depending on the energy dependence of the lead couplings, might have nonzero values.

### 1. $I_{cn}$ : Contributions from residues

As the integrands in Eq. (S8) are of the form  $g(z)/h(z)$ , where  $h$  denotes the denominators of the  $F_n$  functions defined in Eq. (S4), the residues at the simple poles  $z_i$  of  $F_n$ , where  $h(z_i) = 0$ ,  $h'(z_i) \neq 0$  and  $g(z_i) \neq 0$ , can be obtained as  $\text{Res}(g/h, z_i) = g(z_i)/h'(z_i)$ .

$$I_{c1}: F_1(z) = \frac{1}{(z - \Delta_i)^2 + \gamma^2}$$

The function  $F_1$  has simple poles in  $z_i^{\pm} = \Delta_i \pm i\gamma$ ,  $i = 1$  or  $i = 2$ , which contribute to the integrals  $I_{ci}^{\mp}$ , respectively. From the residues we get

$$I_{c1}^{\pm} = \pm 2\pi i \frac{i}{2\pi} \frac{i}{2\gamma} \Gamma_{\alpha}(\Delta_i + \Delta_{mn} \mp i\gamma) \Gamma_{\beta}(\Delta_i \mp i\gamma) \left[ \Psi_{\beta}^{\pm}(\Delta_i \mp i\gamma) - \Psi_{\alpha}^{\pm}(\Delta_i + \Delta_{mn} \mp i\gamma) \right] \quad (\text{S11})$$

The sum of the contributions is

$$\begin{aligned} -I_{c1} &= -I_{c1}^+ - I_{c1}^- = \frac{i}{2\gamma} \left[ \Gamma_{\alpha}(\Delta_i + \Delta_{mn} + i\gamma) \Gamma_{\beta}(\Delta_i + i\gamma) [\Psi_{\alpha}^-(\Delta_i + \Delta_{mn} + i\gamma) - \Psi_{\beta}^-(\Delta_i + i\gamma)] \right. \\ &\quad \left. + \Gamma_{\alpha}(\Delta_i + \Delta_{mn} + i\gamma)^* \Gamma_{\beta}(\Delta_i + i\gamma)^* [\Psi_{\beta}^-(\Delta_i + i\gamma)^* - \Psi_{\alpha}^-(\Delta_i + \Delta_{mn} + i\gamma)^*] \right] \\ &= \frac{1}{\gamma} \text{Im} \left[ \Gamma_{\alpha}(\Delta_i + \Delta_{mn} + i\gamma) \Gamma_{\beta}(\Delta_i + i\gamma) [\Psi_{\beta}^-(\Delta_i + i\gamma) - \Psi_{\alpha}^-(\Delta_i + \Delta_{mn} + i\gamma)] \right] \quad (\text{S12}) \end{aligned}$$

$$= -\frac{1}{\gamma} \text{Im} \left[ \Gamma_{\alpha}(\Delta_i + \Delta_{mn} - i\gamma) \Gamma_{\beta}(\Delta_i - i\gamma) [\Psi_{\beta}^+(\Delta_i - i\gamma) - \Psi_{\alpha}^+(\Delta_i + \Delta_{mn} - i\gamma)] \right], \quad (\text{S13})$$

where we have used the property  $\Psi(z)^* = \Psi(z^*) \rightarrow \Psi^+(z^*) = \Psi^-(z)^*$  of the digamma function.

This contribution diverges when we take the  $\gamma \rightarrow 0$  limit. Following the standard recipe<sup>2,3</sup>, we therefore expand in  $\gamma$ ,  $I_{c1} \approx I_{c1}(\gamma = 0) + \gamma I'_{c1}(\gamma = 0)$ , and discard the diverging  $O(\gamma^{-1})$  term which can be associated with sequential tunneling already included in a separate lowest-order calculation of the tunneling rates. The remaining  $O(\gamma^0)$  term gives the desired contribution to the cotunneling rate,

$$\begin{aligned} -I_{c1}[O(\gamma^0)] &= \text{Re} \left[ [\Gamma'_{\alpha}(\Delta_i + \Delta_{mn}) \Gamma_{\beta}(\Delta_i) + \Gamma_{\alpha}(\Delta_i + \Delta_{mn}) \Gamma'_{\beta}(\Delta_i)] [\Psi_{\beta}^-(\Delta_i) - \Psi_{\alpha}^-(\Delta_i + \Delta_{mn})] \right] \\ &\quad + \frac{\beta}{2\pi} \text{Im} \left[ \Gamma_{\alpha}(\Delta_i + \Delta_{mn}) \Gamma_{\beta}(\Delta_i) [\Psi_{\beta}'^-(\Delta_i) - \Psi_{\alpha}'^-(\Delta_i + \Delta_{mn})] \right], \quad (\text{S14}) \end{aligned}$$

where  $\Gamma'$  denotes the derivative of the lead couplings and  $\Psi'$  is the trigamma function.

$$I_{c2}: F_2(z) = \text{Re} \frac{1}{(z - \Delta_1 + i\gamma)(z - \Delta_2 - i\gamma)}$$

The function  $F_2$  has simple poles in  $z_i^{\pm} = \Delta_i \pm i\gamma$ ,  $i = 1, 2$ , which contribute to the integrals  $I_{c2}^{\mp}$ , respectively. From the residues we get

$$I_{c2}^+ = 2\pi i \frac{i}{2\pi} \text{Re} \frac{1}{\Delta_1 - \Delta_2 - 2i\gamma} \Gamma_{\alpha}(\Delta_1 + \Delta_{mn} - i\gamma) \Gamma_{\beta}(\Delta_1 - i\gamma) \left[ \Psi_{\beta}^+(\Delta_1 - i\gamma) - \Psi_{\alpha}^+(\Delta_1 + \Delta_{mn} - i\gamma) \right] \quad (\text{S15})$$

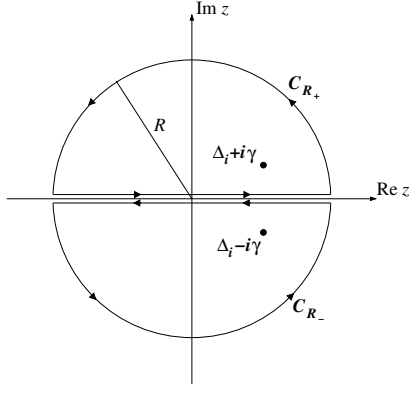


FIG. S2. Integration contours  $C_{\pm}$  for the integrals  $I_n^{\mp}$  in Eq. (S8). The contour integrals are given by the residues at the simple poles  $z_i^{\pm} = \Delta_i \pm i\gamma$  of the  $F_n$  functions defined in Eq. (S4).

and

$$I_{c2}^- = 2\pi i \frac{i}{2\pi} \text{Re} \frac{1}{\Delta_2 - \Delta_1 + 2i\gamma} \Gamma_{\alpha}(\Delta_2 + \Delta_{mn} + i\gamma) \Gamma_{\beta}(\Delta_2 + i\gamma) \left[ \Psi_{\beta}^-(\Delta_2 + i\gamma) - \Psi_{\alpha}^-(\Delta_2 + \Delta_{mn} + i\gamma) \right], \quad (\text{S16})$$

respectively.

The sum of the contributions is

$$\begin{aligned} -I_{c2} &= -I_{c2}^+ - I_{c2}^- = \text{Re} \frac{1}{\Delta_1 - \Delta_2 - 2i\gamma} \left[ \Gamma_{\alpha}(\Delta_1 + \Delta_{mn} - i\gamma) \Gamma_{\beta}(\Delta_1 - i\gamma) [\Psi_{\beta}^+(\Delta_1 - i\gamma) - \Psi_{\alpha}^+(\Delta_1 + \Delta_{mn} - i\gamma)] \right. \\ &\quad \left. - \Gamma_{\alpha}(\Delta_2 + \Delta_{mn} + i\gamma) \Gamma_{\beta}(\Delta_2 + i\gamma) [\Psi_{\beta}^-(\Delta_2 + i\gamma) - \Psi_{\alpha}^-(\Delta_2 + \Delta_{mn} + i\gamma)] \right] \\ &\stackrel{\gamma \rightarrow 0}{=} \frac{1}{\Delta_1 - \Delta_2} \text{Re} \left[ \Gamma_{\alpha}(\Delta_1 + \Delta_{mn}) \Gamma_{\beta}(\Delta_1) [\Psi_{\beta}^+(\Delta_1) - \Psi_{\alpha}^+(\Delta_1 + \Delta_{mn})] \right. \\ &\quad \left. - \Gamma_{\alpha}(\Delta_2 + \Delta_{mn}) \Gamma_{\beta}(\Delta_2) [\Psi_{\beta}^-(\Delta_2) - \Psi_{\alpha}^-(\Delta_2 + \Delta_{mn})] \right]. \end{aligned} \quad (\text{S17})$$

Here we do not encounter any problems taking the  $\gamma \rightarrow 0$  limit.

## 2. $I_{C_{Rn}}$ : Contributions from semi-circle arcs

In order to calculate the contributions from the integrals along the semi-circle arcs in the limit  $R \rightarrow \infty$ , we use the asymptotic expansion of the digamma function<sup>5</sup>

$$\lim_{|z| \rightarrow \infty} \Psi(z) = -\gamma + \sum_{n=1}^{\infty} \frac{z}{n(n+z)} = \ln z - \frac{1}{2z} - \sum_{n=1}^{\infty} \frac{B_{2n}}{2nz^{2n}}, \quad (\text{S18})$$

where  $\gamma$  is the Euler-Mascheroni constant and  $B_{2n}$  are Bernoulli numbers. From the asymptotic expansion, we find for the factors in Eq. (S8) involving the  $\Psi^{\pm}$  functions

$$\begin{aligned} \lim_{|z| \rightarrow \infty} \left[ \Psi_{\beta}^+(z) - \Psi_{\alpha}^+(z + \Delta_{mn}) \right] &= \ln \left[ 1 + \frac{i\beta}{2\pi} \frac{\mu_{\alpha} - \mu_{\beta} - \Delta_{mn}}{1/2 + i\beta/2\pi(z + \Delta_{mn} - \mu_{\alpha})} \right] - \frac{1}{1 + i\beta(z - \mu_{\beta})/\pi} + \frac{1}{1 + i\beta(z + \Delta_{mn} - \mu_{\alpha})/\pi} + \dots \\ &\approx \ln \left[ 1 + \frac{\mu_{\alpha} - \mu_{\beta} - \Delta_{mn}}{z} \right] + i \frac{\mu_{\beta} - \mu_{\alpha} + \Delta_{mn}}{\beta z^2/\pi} + \dots \\ &\approx \frac{\mu_{\alpha} - \mu_{\beta} - \Delta_{mn}}{z} \end{aligned} \quad (\text{S19})$$

and

$$\begin{aligned}
\lim_{|z| \rightarrow \infty} \left[ \Psi_{\beta}^{-}(z) - \Psi_{\alpha}^{-}(z + \Delta_{mn}) \right] &= \ln \left[ 1 - \frac{i\beta}{2\pi} \frac{\mu_{\alpha} - \mu_{\beta} - \Delta_{mn}}{1/2 - i\beta/2\pi(z + \Delta_{mn} - \mu_{\alpha})} \right] - \frac{1}{1 - i\beta(z - \mu_{\beta})/\pi} + \frac{1}{1 - i\beta(z + \Delta_{mn} - \mu_{\alpha})/\pi} + \dots \\
&\approx \ln \left[ 1 + \frac{\mu_{\alpha} - \mu_{\beta} - \Delta_{mn}}{z} \right] - i \frac{\mu_{\alpha} - \mu_{\beta} - \Delta_{mn}}{\beta z^2/\pi} + \dots \\
&\approx \frac{\mu_{\alpha} - \mu_{\beta} - \Delta_{mn}}{z},
\end{aligned} \tag{S20}$$

respectively.

In addition we have that  $\lim_{|z| \rightarrow \infty} F_n(z) = z^{-2}$ . Inserting in Eq. (S8) with  $z = Re^{i\theta} \rightarrow dz = iRe^{i\theta}d\theta$  on the semi-circle arcs, we find

$$\begin{aligned}
I_{C_R n} &= I_{C_{R-}}^{+} + I_{C_{R+}}^{-} \\
&= \frac{i^2}{2\pi} \int_{-\pi}^0 d\theta Re^{i\theta} \Gamma_{\alpha}(Re^{i\theta}) \Gamma_{\beta}(Re^{i\theta}) \frac{1}{R^2 e^{2i\theta}} \frac{\mu_{\alpha} - \mu_{\beta} - \Delta_{mn}}{Re^{i\theta}} \\
&\quad + \frac{i^2}{2\pi} \int_0^{\pi} d\theta Re^{i\theta} \Gamma_{\alpha}(Re^{i\theta}) \Gamma_{\beta}(Re^{i\theta}) \frac{1}{R^2 e^{2i\theta}} \frac{\mu_{\alpha} - \mu_{\beta} - \Delta_{mn}}{Re^{i\theta}} \\
&= \frac{\mu_{\beta} - \mu_{\alpha} + \Delta_{mn}}{2\pi} \int_{-\pi}^{\pi} d\theta \frac{\Gamma_{\alpha}(Re^{i\theta}) \Gamma_{\beta}(Re^{i\theta})}{R^2 e^{2i\theta}}
\end{aligned} \tag{S21}$$

Thus, as long as the asymptotic behavior of the lead couplings is  $\lim_{|z| \rightarrow \infty} \Gamma_{\alpha}(z) = z^n$  with  $n < 1$ , the integrals along the semi-circle arcs vanish for  $R \rightarrow \infty$ . For graphene leads, this is not the case (see below).

It should be noted that for  $A = -B$ , i.e. with one electron- and one hole-like intermediate state, the semi-circle contributions from the different terms in Eq. (S2) cancel in the cotunneling rate.

## B. Linearized lead couplings

At low bias (compared to the energy scale at which the lead couplings show nonlinear energy dependence), we can expand the lead couplings around the equilibrium chemical potentials  $\mu_0$  of the leads,  $\Gamma_{\alpha}(\varepsilon) \approx \Gamma_{\alpha 0} + \xi \partial \Gamma_{\alpha}$ , where  $\xi = \varepsilon - \mu_0$ ,  $\Gamma_{\alpha 0} = \Gamma_{\alpha}(\mu_0)$ , and  $\partial \Gamma_{\alpha} = \partial \Gamma_{\alpha} / \partial \varepsilon|_{\varepsilon = \mu_0}$ . With this approximation,  $\lim_{|z| \rightarrow \infty} \Gamma_{\alpha}(z) = z \partial \Gamma_{\alpha}$ , and the integrals along the semi-circle arcs in Eq. (S21) attain a finite value,

$$I_{C_R n} = \partial \Gamma_{\alpha} \partial \Gamma_{\beta} (\mu_{\beta} - \mu_{\alpha} + \Delta_{mn}). \tag{S22}$$

It should be pointed out that the apparent contradiction associated with the fact that we here have used the  $|z| \rightarrow \infty$  limit of an expansion valid at low energies only, is both physically and mathematically sound. The integral along the real axis in Eq. (S1) [and Eq. (S7)] is cut off by the Fermi functions and does *not* depend on the behavior of the lead couplings at  $\varepsilon \rightarrow \infty$ . Only when the real-axis integrals in Eq. (S7) are expressed in terms of the different contributions to the contour integrals in Eq. (S8), as in Eq. (S10), does the  $z \rightarrow \infty$  limit of the lead couplings enter.

### Graphene leads

For bulk graphene leads with linear DOS,  $\rho(\varepsilon) \propto |\varepsilon|$ , the lead couplings acquire the linear energy dependence of the DOS if the tunnel couplings are assumed independent on energy, i.e.  $\Gamma(\varepsilon) \propto \rho(\varepsilon)$ . In this case the result in Eq. (S22) above applies. However, it should be noted that, as the graphene DOS is nonanalytic at the Dirac point where the DOS vanishes, the result obtained here strictly only holds away from the Dirac point.

---

\* cosby@fys.ku.dk

<sup>1</sup> S. Amasha, A. J. Keller, I. G. Rau, A. Carmi, J. A. Katine, H. Shtrikman, Y. Oreg, and D. Goldhaber-Gordon, Phys. Rev. Lett. **110**, 046604 (2013).

<sup>2</sup> M. Turek and K. A. Matveev, Phys. Rev. B **65**, 115332 (2002).

- <sup>3</sup> J. Koch, F. von Oppen, Y. Oreg, and E. Sela, *Phys. Rev. B* **70**, 195107 (2004).
- <sup>4</sup> H. Bruus and K. Flensberg, *Many-body Quantum Theory in Condensed Matter Physics* (Oxford University Press, 2004).
- <sup>5</sup> M. Abramowitz and I. A. Stegun, *Handbook of Mathematical Functions with Formulas, Graphs, and Mathematical Tables*, 10th ed. (Dover, New York, 1964).